Journal of
Synchrotron
Radiation

ISSN 0909-0495

Received 23 September 2009
Accepted 2 September 2010

# Hard X-ray imaging for landslide research

B. M. Weon,[a,b]* J. H. Je[b]* and G. Gremaud[c]

[a]Department of Physics, School of Engineering and Applied Sciences, Harvard University, Cambridge, MA 02138, USA, [b]X-ray Imaging Center, Department of Materials Science and Engineering, Pohang University of Science and Technology, Pohang 790-784, Republic of Korea, and [c]Institut de Physique de la Matière Complexe, Ecole Polytechnique Fédérale de Lausanne (EPFL), CH-1015 Lausanne, Switzerland. E-mail: bmweon@seas.harvard.edu, jhje@postech.ac.kr

Synchrotron phase-contrast hard X-ray imaging is used to provide highly efficient direct visualization of landslide dynamics and granular flows in fully wet granular piles. High penetration capability and phase-contrast enhancement of hard X-rays offer marked advantages in the precise tracking of individual granular movements through a thick water medium. It is revealed that the stress accumulation follows a power-law evolution while the relaxation follows an exponential one. The onset of landslide emerges at the trade-off of the two evolutions.



**Keywords: hard X-rays; landslides; real-time imaging; granular displacements.**

## 1. Introduction

Direct visualization of flows in realistic granular materials is an important problem from both a practical and theoretical point of view. Granular materials play an important role in geological processes such as landslides and erosion that determine much of Earth's morphology (Jaeger *et al.*, 1996*a*). Water significantly affects the stability of granular materials. As commonly observed when building a sandcastle, water in partly wet sandpiles produces cohesion between grains by capillary bridges (Webster, 1919; Jaeger *et al.*, 1996*b*; Hornbaker *et al.*, 1997; Halsey & Levine, 1998; Kudrolli, 2008; Scheel *et al.*, 2008). In fully wet piles, however, water induces natural landslides (Nisbet & Piper, 1998; Hilley *et al.*, 2004; Herminghaus, 2005; Mitarai & Nori, 2006; Keefer & Larsen, 2007) by no cohesion (Tegzes *et al.*, 2002; Courrech du Pont *et al.*, 2003; Schiffer, 2005; Nowak *et al.*, 2005). Understanding how landslides evolve in fully wet piles is still a significant problem. The stability of the sandpile directly correlates with landslide evolution, which is dynamic and very sensitive to natural or artificial perturbations. After the primitive study on water-induced sandpile stability by Webster (1919), many efforts have been devoted to exploring the singularities of granular pile stability. The underlying physics for the stability of dry or partly wet granular piles has been well understood over the last decades (Jaeger *et al.*, 1996*b*; Hornbaker *et al.*, 1997; Halsey & Levine, 1998; Tegzes *et al.*, 2002; Courrech du Pont *et al.*, 2003; Schiffer, 2005; Nowak *et al.*, 2005). However, an understanding of granular flows or completely wet granular piles (or slurries) remains lacking (Courrech du Pont *et al.*, 2003). Direct visualization of granular flows is essential to study landslide dynamics and statistics for fully wet granular piles.

In this work we present a useful experimental approach of synchrotron phase-contrast hard X-ray imaging (Snigirev *et al.*, 1995; Nugent *et al.*, 1996; Wilkins *et al.*, 1996; Cloetens *et al.*, 1996; Tsai *et al.*, 2002). High penetration capability and phase-contrast enhancement of hard X-rays from a synchrotron source (the PLS 7B2 beamline in Pohang, Korea) (Weon *et al.*, 2006, 2008*a*,*b*,*c*) may offer marked advantages in the precise tracking of granular movements through a thick water medium compared with conventional absorption-based X-ray techniques (Royer *et al.*, 2005).

Our approach may have a straightforward impact on the understanding of natural events such as rainfall-induced landslides (Hilley *et al.*, 2004; Herminghaus, 2005; Mitarai & Nori, 2006) or submarine landslides (Nisbet & Piper, 1998; Keefer & Larsen, 2007), which may occasionally generate tsunamis. The basic physics governing the initiation of landslides has long been studied but the catastrophic features are little understood (Keefer & Larsen, 2007). One of the reasons for this is the difficult visualization of landslide dynamics (Hilley *et al.*, 2004). Our X-ray imaging approach enables us to track granular displacements and helps to understand how underwater landslides break out and evolve.

## 2. Experimental

The experimental set-up of underwater landslides, as illustrated in Fig. 1(*a*), consists of a pile of spherical microspheres completely immersed in water. We tested four different microspheres: polymethylmethacrylate (PMMA), polystyrene, silica and real sand. Initially microspheres are piled in a corner by inclining a rectangular container. After complete sedimentation, the container is returned to the original angle.

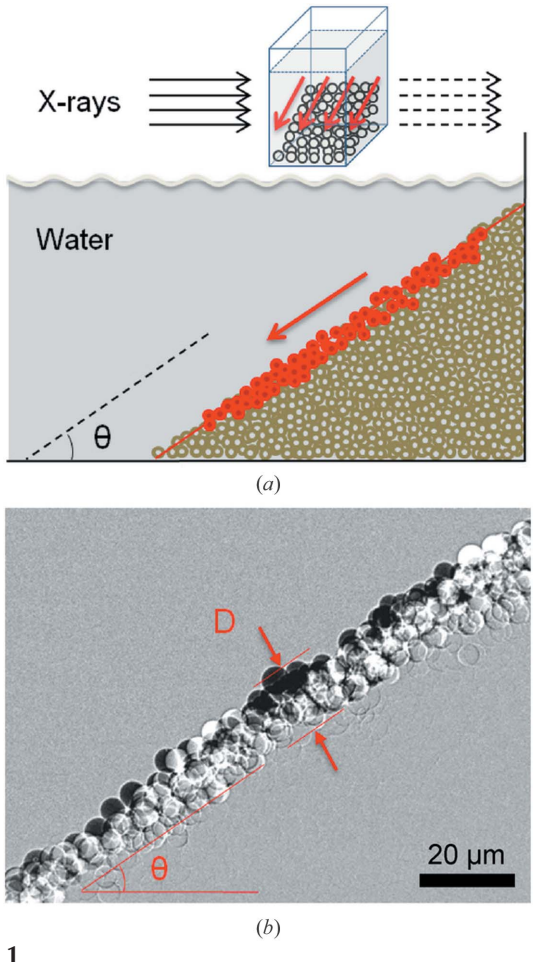


**Figure 1**
(*a*) Top: experimental set-up for observation of landslide events in a thick medium. Bottom: diagram of underwater landslide events. (*b*) Visualization of granular displacements at a sliding surface with sliding depth $D$ and sliding angle $\theta$, clearly showing the landslide dynamics.

Natural sliding events on the slope are visualized by X-ray imaging. Sufficiently large sizes of grains (diameter $d$) are chosen to neglect thermally induced Brownian motion compared with gravitational sedimentation. A quasi-two-dimensional container (10 mm length, 100 mm height and a width larger than $\sim 20d$) is used to reduce side wall effects on the stability (wall effects may still exist). Optimizing phase-contrast enhancement enables us to clearly visualize the details of sliding dynamics at an inclination angle $\theta$.

Spatially coherent synchrotron hard X-rays in the 10–60 keV photon energy band with a centroid of 20 keV for 1 mm-thick Si attenuators (Baik *et al.*, 2004) are used to track the detailed granular movements on a slope in real time using a $CdWO_4$ scintillator crystal and a CCD (charge-coupled device) camera. The scintillator–specimen distance is set at 150 mm to optimize phase-contrast enhancement. The beam cross section is tuned to 0.58 mm × 0.44 mm and the micro-radiology spatial resolution is 0.5 μm. Sequential micro-radiographs are taken with an interval time (acquisition time of 100 ms and data transmission time of 400 ms). Sequential snapshots in movies were treated using the *Image-Pro Plus* software (MediaCybernetics).

A representative direct visualization of mobile granular displacements on the sliding surface is illustrated in Fig. 1(*b*), which was obtained by subtracting two sequential images taken at an interval of 0.5 s. The mobile grains on the slope surface are clearly differentiated from the immobile grains of the bulk region: white (black) circles indicate sites vacated (occupied) by moved grains. X-ray imaging enables us to measure the sliding depth $D$ and the sliding angle $\theta$ which are two critical parameters for characterizing the granular displacements in completely wet granular piles.

## 3. Results and discussion

To study the evolution of a single sliding event collectively, we use a large amount of PMMA microspheres of diameter 6.5 μm (density 1.19 g cm$^{-3}$). The evolution of the granular displacements at time $t$ is illustrated in Fig. 2, obtained by subtracting the initial image at time $t_0$ from the images at time $t$. All images were taken in a single X-ray movie. Interestingly we see that the sliding depth (indicated by the open red arrows) initially propagates with time and saturates to $\sim 18d$ after ∼25 s. On the other hand the sliding angle (indicated by the closed yellow arrows) keeps constant at $\sim 18^\circ$ up to 25 s, but gradually decreases to $\sim 1^\circ$ in later stages. These results suggest two distinct landslide mechanisms in fully wet granular piles.

The time evolutions of the sliding depth $D$ and the sliding angle $\theta$ are plotted in Fig. 3. The propagation depth $N$ (= $D/d$; the sliding depth divided by the particle diameter $d$) and the sliding angle $\theta$ were measured from the sequential images of Fig. 2. Granular displacements indicate stress evolution. Two distinct regimes are immediately shown in Fig. 3. In the first regime ($t < 25$ s) the propagation depth $N$ grows steeply with time by a power-law scaling $N \simeq t^{\delta}$ while the sliding angle $\theta$ is almost invariant ($\sim 18^\circ$). A quarter power-law scaling ($\delta \simeq 1/4 \pm 0.01$) is found in the $\log N$–$\log t$ plot. This specific scaling has not been reported until recently. On the other hand the almost constant sliding angle in the first regime indicates stress accumulation in the sliding depth. In the second regime ($t >$ 25 s) the sliding angle drastically changes, indicating stress relaxation, which is similar to dry granular beads in rotating drums (Courrech du Pont *et al.*, 2005). The angle decreases exponentially with time, $\theta \simeq \exp(-\lambda t)$, at a constant decay rate $\lambda$.

The quarter power-law in the first regime and the simple exponential scaling in the second regime strongly suggest two distinct physical mechanisms underlying the granular displacements. Very importantly we note that the onset of the slide appears right at the trade-off between the two distinct dynamics of $N \simeq t^{1/4}$ (stress accumulation) and $\theta \simeq \exp(-\lambda t)$ (stress relaxation).

For a quantitative understanding, let us imagine fragile grains on a slope ($\theta$) with a volume $V = wd^2N^2\theta^{-1}$ which consists of height $D$ (= $Nd$) and base $D(\tan\theta)^{-1}$ for a constant container width ($w$) and small angle approximation ($\tan\theta \simeq \theta$). The fragile volume is given as $V \propto N^2\theta^{-1}$. This suggests that the fragile volume builds up as $V \propto t^{1/2}$ for constant $\theta$ and then

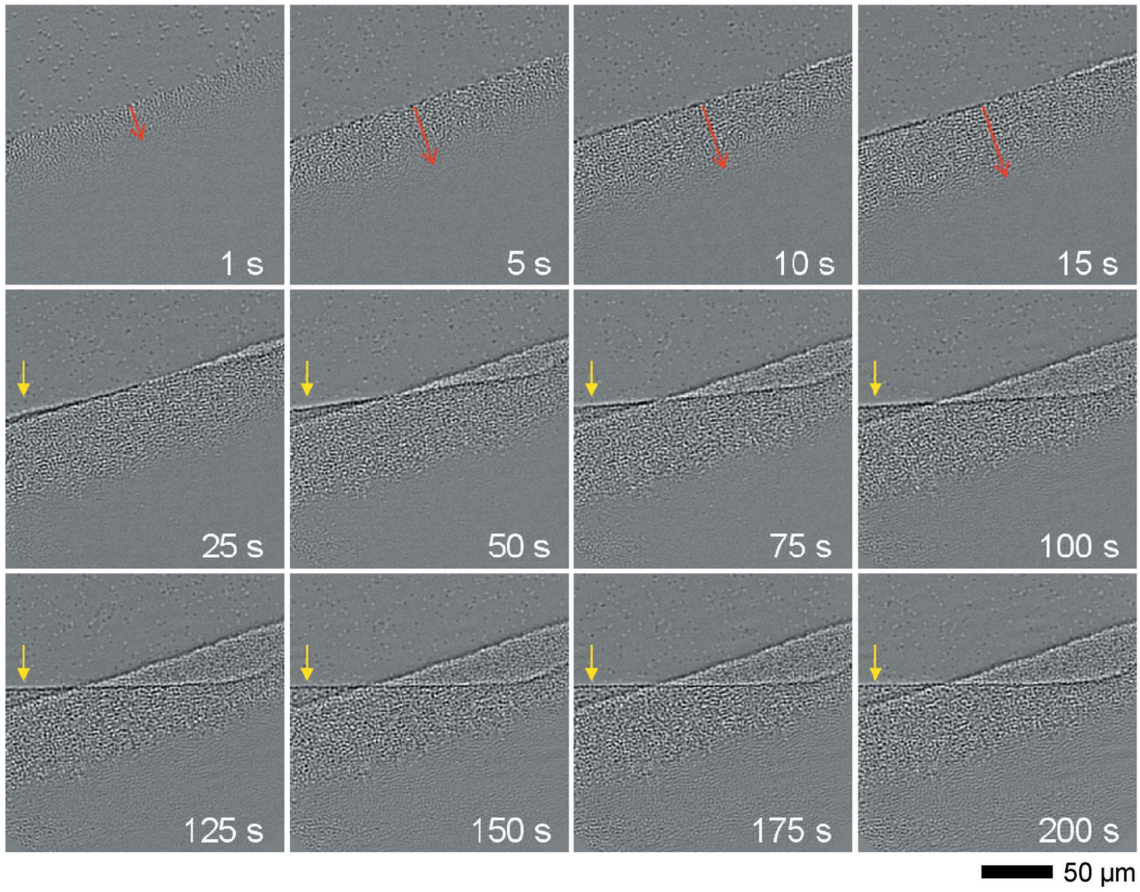


**Figure 2**
Sequential images of a single sliding event taken from a pile of PMMA microspheres by subtracting the initial image at time $t_0$ from the images at time $t$. The sliding depth (open red arrows) propagates with time up to 25 s while the sliding angle (closed yellow arrows) decreases after 25 s, suggesting two distinct mechanisms.

vanishes as $V \propto \exp(\lambda t)$ for constant $N$. The physical explanation remains an open debate. Further studies may be designed to clarify the origin of the two distinct dynamics, to verify the buoyant effect or the viscosity effect in various liquids, and to compare wet piles with dry piles. The explanation of these two regimes and their dynamics will be a puzzling problem for theorists; in particular, the fact that the large slope difference ($\Delta\theta$) between the onset (18°) and the end (1°) slopes (Fig. 2) is pertinent to the situations in which granular piles under water are very fragile to perturbations and prone to have gentle slopes. The large $\Delta\theta$ is attributable to the fragility in grains of small sizes, which make grains sensitive to sedimentation conditions or particle interactions. For heavy or large grains $\Delta\theta$ is small, similar to typical drum cases (Courrech du Pont *et al.*, 2003).

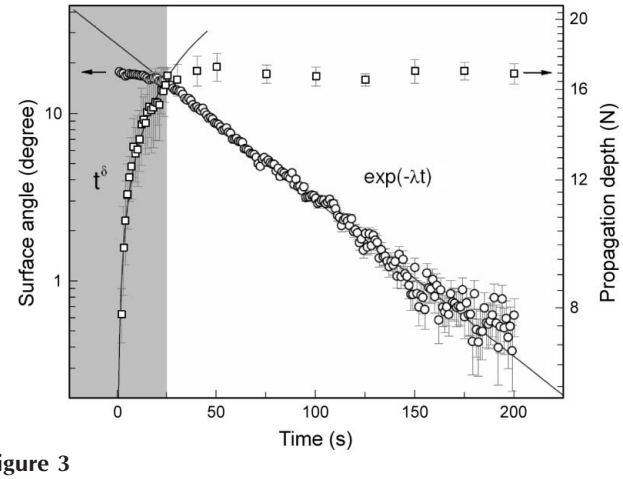


**Figure 3**
Propagation depth and sliding angle (Fig. 2) as a function of time. The propagation depth $N$ (squares) grows by a power-law scaling as $N \simeq t^{\delta}$ before 25 s (grey) and the surface angle (circles) decreases exponentially with time as $\theta \simeq \exp(-\lambda t)$ after 25 s.

The sliding mode is significantly different for light and heavy grains. Specifically we tested polystyrene (1.05 g cm$^{-3}$) and silica (2.20 g cm$^{-3}$) grains of the same size, ∼50 µm (with sphericity >98%, coefficient of friction 0.5–0.9 from bulk materials, and size polydispersity <5%). The sliding angle was 'gentle' (∼2°) and the sliding flow was 'continuous' for the light grains, while 'steep' (∼30°) and 'discrete' for the heavy grains (data not shown). The continuous gentle sliding for the light grains is attributed to their low friction in water from the buoyant effect. The friction reduction in the heavy grains is relatively small, resulting in discrete steep sliding, similar to that observed in dry piles. For real sand we see the discrete steep sliding behaviour like for the silica grains. These results

imply that the grain properties would affect the sliding dynamics, invoking further studies about other effects such as inhomogeneity in size and minimization of edge effects (grain-wall interactions).

Our discoveries may help further experimental or theoretical studies on landslide dynamics (Pailha *et al.*, 2008). The stress evolution dynamics suggest that small events, triggered by small stresses, occur more frequently than large events by self-organized criticality (Bak *et al.*, 1987, 1988). High-resolution monitoring of landslides is important for studying landslide dynamics and statistics (Iverson, 1997; Oppikofer *et al.*, 2008). Synchrotron phase-contrast hard X-ray imaging would have advantages in solving long-standing problems in geophysical events (Bleuet *et al.*, 2008) and in instabilities of suspensions with athermal grains (Forterre & Pouliquen, 2008).

## 4. Conclusion

We have shown that synchrotron phase-contrast hard X-ray imaging can provide highly efficient direct visualization of landslide dynamics and granular flows in fully wet granular piles, thanks to the high penetration capability and phase-contrast enhancement of hard X-rays. Precise tracking of individual granular movements through a thick water medium shows that the accumulation of stress follows a power-law evolution and the relaxation an exponential evolution, and the onset of landslide emerges at a trade-off between the two evolutions. Generally speaking, synchrotron phase-contrast hard X-ray imaging would offer a better understanding of underwater granular systems regarding many important physical and geophysical problems.

This research was supported by the Creative Research Initiatives (Functional X-ray Imaging) of MEST/NRF.

## References

Baik, S., Kim, H. S., Jeong, M. H., Lee, C. S., Je, J. H., Hwu, Y. & Margaritondo, G. (2004). *Rev. Sci. Instrum.* **75**, 4355–4358.
Bak, P., Tang, C. & Wiesenfeld, K. (1987). *Phys. Rev. Lett.* **59**, 381–384.
Bak, P., Tang, C. & Wiesenfeld, K. (1988). *Phys. Rev. A*, **38**, 364–374.
Bleuet, P., Simionovici, A., Lemelle, L., Ferroir, T., Cloetens, P., Tucoulou, R. & Susini, J. (2008). *Appl. Phys. Lett.* **92**, 213111.
Cloetens, P., Barrett, R., Baruchel, J., Guigay, J. P. & Schlenker, M. (1996). *J. Phys. D*, **29**, 133–146.
Courrech du Pont, S., Fischer, R., Gondret, P., Perrin, B. & Rabaud, M. (2005). *Phys. Rev. Lett.* **94**, 048003.
Courrech du Pont, S., Gondret, P., Perrin, B. & Rabaud, M. (2003). *Phys. Rev. Lett.* **90**, 044301.
Forterre, Y. & Pouliquen, O. (2008). *Annu. Rev. Fluid Mech.* **40**, 1–24.
Halsey, T. C. & Levine, A. J. (1998). *Phys. Rev. Lett.* **80**, 3141–3144.
Herminghaus, S. (2005). *Adv. Phys.* **54**, 221–261.
Hilley, G. E., Bürgmann, R., Ferretti, A., Novali, F. & Rocca, F. (2004). *Science*, **304**, 1952–1954.
Hornbaker, D., Albert, R., Albert, I., Barabási, A. L. & Schiffer, P. (1997). *Nature (London)*, **387**, 765.
Iverson, R. M. (1997). *Rev. Geophys.* **35**, 245–296.
Jaeger, H. M., Nagel, S. R. & Behringer, R. P. (1996*a*). *Phys. Today*, **49**, 32–38.
Jaeger, H. M., Nagel, S. R. & Behringer, R. P. (1996*b*). *Rev. Mod. Phys.* **68**, 1259–1273.
Keefer, D. K. & Larsen, M. C. (2007). *Science*, **316**, 1136–1138.
Kudrolli, A. (2008). *Nat. Mater.* **7**, 174–175.
Mitarai, N. & Nori, F. (2006). *Adv. Phys.* **55**, 1–45.
Nisbet, E. & Piper, D. J. W. (1998). *Nature (London)*, **392**, 329–330.
Nowak, S., Samadani, A. & Kudrolli, A. (2005). *Nat. Phys.* **1**, 50–52.
Nugent, K. A., Gureyev, T. E., Cookson, D., Paganin, D. & Barnea, Z. (1996). *Phys. Rev. Lett.* **77**, 2961–2964.
Oppikofer, T., Jaboyedoff, M. & Keusen, H.-R. (2008). *Nat. Geosci.* **1**, 531–535.
Pailha, M., Nicolas, M. & Pouliquen, O. (2008). *Phys. Fluids*, **20**, 111701.
Royer, J. R., Corwin, E. I., Flior, A., Cordero, M.-L., Rivers, M. L., Eng, P. J. & Jaeger, H. M. (2005). *Nat. Phys.* **1**, 164–167.
Scheel, M., Seemann. R., Brinkmann, M., Michiel. M. D., Sheppard, A., Breidenbach, B. & Herminghaus, S. (2008). *Nat. Mater.* **7**, 189–193.
Schiffer, P. (2005). *Nat. Phys.* **1**, 21–22.
Snigirev, A., Snigireva, I., Kohn, V., Kuznetsov, S. & Schelokov, I. (1995). *Rev. Sci. Instrum.* **66**, 5486–5492.
Tegzes, P., Vicsek, T. & Schiffer, P. (2002). *Phys. Rev. Lett.* **89**, 094301.
Tsai, W. L., Hsu, P. C., Hwu, Y., Chen, C. H., Chang, L. W., Je, J. H., Lin, H. M., Groso, A. & Margaritondo, G. (2002). *Nature (London)*, **417**, 139.
Webster, A. G. (1919). *Proc. Natl. Acad. Sci. USA*, **5**, 263–265.
Weon, B. M., Je, J. H., Hwu, Y. & Margaritondo, G. (2006). *Int. J. Nanotechnol.* **3**, 280–297.
Weon, B. M., Je, J. H., Hwu, Y. & Margaritondo, G. (2008*a*). *Phys. Rev. Lett.* **100**, 217403.
Weon, B. M., Je, J. H., Hwu, Y. & Margaritondo, G. (2008*b*). *Appl. Phys. Lett.* **92**, 104101.
Weon, B. M., Je, J. H., Hwu, Y. & Margaritondo, G. (2008*c*). *J. Synchrotron Rad.* **15**, 660–662.
Wilkins, S. W., Gureyev, T. E., Gao, D., Pogany, A. & Stevenson, A. W. (1996). *Nature (London)*, **384**, 335–338.